Archives of Hydro-Engineering and Environmental Mechanics
Vol. 55 (2008), No. 3–4, pp. 125–143

Experimental Analysis of Relations Between Coherent Turbulent Structures and Formation of Bedforms

Donatella Termini, Vincenzo Sammartano

Dipartimento di Idraulica ed Applicazioni Ambientali, Facoltà di Ingegneria, Università di Palermo, Italy, phone: ++39 0916557722; fax: ++39 0916557749; e-mails: dony@idra.unipa.it; sammartano@idra.unipa.it

(Received February 05, 2009; revised March 16, 2009)

Abstract

The present paper describes an experimental investigation on the interactions between flow turbulence and sediment motion. During the experiments, detailed measurements of flow velocity components were carried out using an Acoustic Doppler Velocimeter (ADV). The occurrence of turbulent events (inward interaction, ejection, sweep and burst) was verified through conditioned quadrant analysis. The quantitative information on the spatial and temporal evolution of turbulent events was obtained through space-time correlations of the conditioned data. As the primary objective was to analyse how turbulent structures influence formation of bedforms, the spatial scale of turbulent event evolution has been compared with the wavelength of bed-forms (alternate bars) observed on the bed. The analysis has essentially highlighted that such spatial scale compares well with the wavelength of the bars.

Key words: open channel flow, sediment transport, bedforms, flow turbulence structure

List of Symbols

D_{50} – median sediment diameter (mm),
f_k – occurrence frequency of the event falling in k-th quadrant,
F – frequency of the calculated points in FFT (Hz),
F_n – normalized frequency,
F_s – sampling frequency (Hz),
I_k – discriminating function,
$N_{k,z}$ – number of occurrences of turbulent event in k-th quadrant,
P_{12} – joint probability density of filtered turbulent components,
q – threshold level,
S_0 – initial section,
S – detected section,
t – time (sec),
T – measurement time length (sec),

$u_1(z,t)$ – instantaneous stream-wise velocity component at distance z from the bed (cm/s),
$u_2(z,t)$ – instantaneous transverse velocity component at distance z from the bed (cm/s),
$u_1'(z,t)$ – stream-wise instantaneous turbulent fluctuation component at distance z from the bed (cm/s),
$u_2'(z,t)$ – transverse instantaneous turbulent fluctuation component at distance z from the bed (cm/s),
$\hat{u}_1'(z,t)$ – filtered stream-wise instantaneous turbulent fluctuation component at distance z from the bed (cm/s),
$\hat{u}_2'(z,t)$ – filtered transverse instantaneous turbulent fluctuation component at distance z from the bed (cm/s),
$u_1'u_2'$ – instantaneous Reynolds stress,
$U_1(z)$ – time averaged of stream-wise velocity component at distance z from the bed (cm/s),
z – distance of measurement point from the bed (cm),
ρ_{12} – correlation coefficient between filtered stream-wise and transverse turbulent components,
σ_g – sediment geometric standard deviation,
Δx – spatial lag (cm),
τ – time lag (sec).

1. Introduction

The prediction of shape and size of migrating bed forms is an object of study in such disciplines as geomorphology, hydraulics and sedimentology. Even today, understanding of flow-bed coupling is insufficient to produce predictive models for generation of bedforms.

The mechanics of sediment transport is strongly related to wall layer flow characteristics and turbulent processes. In fact, bed-forms are generated by flow and they, in turn, significantly modify local flow and turbulence fields (Nelson et al 1995, Holmes and Garcia 2008).

As experimental and theoretical studies show (Nezu and Rodi 1986, Nezu and Nakagawa 1993, Shvidchenko and Pender 2001), the dynamics of wall layer turbulence is dominated by the formation and growth of turbulent structures, called coherent structures, which evolve periodically as part of the so-called bursting phenomena. These phenomena consist of four phases: inward interaction, ejection, sweep, and outward interaction (Kline et al 1967, Corino and Brodkey 1969, Jackson 1976, Cantwell 1981). During the first phase (inward interaction), streaks of low-speed fluid migrate slowly away from the wall, rolling up into an eddy; then, at a certain point, they turn and move away from the wall rapidly (ejection); during the ejection, high-speed fluid regions move toward the wall passing under the eddy

(sweep), until the eddy is conveyed downstream with a rapid oscillation; such oscillation is followed by a breakdown into finer-scale motion (outward interaction). Thus, the small-scale coherent eddy structure (inner region) arises from the wall, developing into a large-scale eddy (outer region) and influencing the large-scale turbulent structure of flow (Nezu and Nakagawa 1993). Ejection and sweep events, which contribute positively to Reynolds shear stress, seem to play the most important role in erosion, entrapment and transport of sediment particles (Jackson 1976, Rashidi et al 1990, Kaftori et al 1995, Nino and Garcia 1996, Shen and Lemmin 1999).

The bursting sequences could be both "vertical" (i.e. formed by eddies whose axes of rotation are perpendicular to the vertical plane) and "horizontal" (i.e. formed by eddies whose axes of rotation are perpendicular to the horizontal plane) (Utami and Ueno 1991, Yalin 1992).

Most studies analyse the relation between the evolution of the "vertical" bursting sequences and the formation of some bed-forms as ripples and dunes. Nelson et al (1995) conducted a series of experiments, in a straight laboratory channel, to investigate the interaction between near-bed turbulence and sediment movement in a spatially non-uniform flow, as observed over the aforementioned bed-forms. Nelson et al (1995) verified that the "vertical" turbulent structures associated with the separation and reattachment processes downstream of the bed-form crest affect the sediment transport field. In fact, the high-magnitude and low frequency turbulence events enhance the entrapment and movement of sediment grains.

Recent experimental investigations conducted in a straight laboratory channel with alternate bars on the bed (Termini 2005, Termini and Lo Re 2006), have also verified the existence of a relation between the occurrence of "horizontal" turbulent structures and bar development. Further experimental results obtained by Termini and Sammartano (2007) in the same laboratory channel, but with a flat bed, have supported the idea that alternate bars initiate due to "horizontal bursts", in accordance with other researchers (Yalin 1992, Yalin and da Silva 2001, da Silva 2006).

The aim of the present work is to further understanding about "horizontal" turbulent events and to verify how their development could influence initiation of alternate bars. The statistics of ejection and sweep dynamics are determined and analyzed in different locations along the considered straight flume.

2. Experimental Data

The experimental data were collected during experiments carried out in a rectangular straight flume, constructed at the laboratory of Dipartimento di Ingegneria Idraulica ed Applicazioni Ambientali – University of Palermo (Italy). The plane view of the experimental apparatus is given in Fig. 1. The channel is 0.40 m wide and 7 m long. The channel banks are rigid and realized with Plexiglas streaks; the

bed is of quartz sand (D_{50} = 0.65 mm, σ_g = 1.334, with D_{50} = median sediment diameter and σ_g = geometric standard deviation). A pumping tank is at the downstream end of the channel and an hydraulic circuit, connecting the outlet and the inlet structures of the flume, allows a continuous recirculation of both the stable discharge and the sand. Two experimental runs have been conducted under steady flow conditions: mobile-bed and rigid-flat-bed runs. For the mobile-bed run, the bed of the channel was rigid only in the upstream reach 1 m long (see Fig. 1).

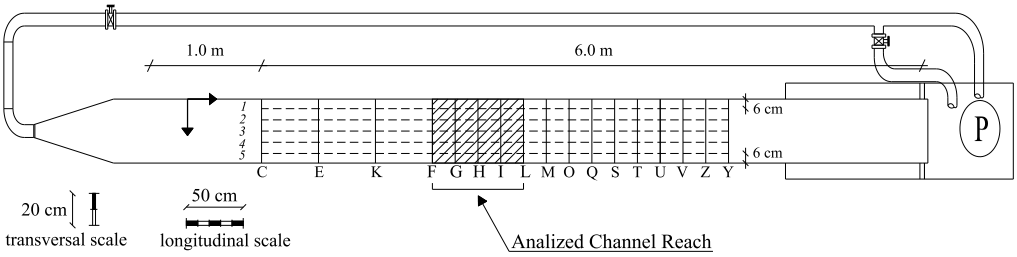

Fig. 1. Plane view of the experimental apparatus

For both runs, the water discharge was of 0.013 m^3/s and the initial bed slope was of 0.45%. First, the mobile-bed experiment was carried out until to reach the equilibrium bed configuration. During the experiment, the evolution of the bed deformation was measured through a profile indicator by Delft Hydraulics (with precision of 0.1 mm) along the longitudinal measurement axes 1–5 shown in Fig. 1. The longitudinal measurement axes were spaced 7 cm apart; both axes 1 and 5 were a distance of 6 cm from the wall (see Fig. 1). As Fig. 2 shows, at the end of the experiment, the bed was covered with double row alternate bars having wavelength of about 0.80 ÷ 0.90 m. As reported in a previous work (Termini and Lo Re 2006), the spatial and temporal description of bed-form evolution was obtained through analysis, in temporal and in spatial domains, of the self-correlation functions of the measured instantaneous bed level data.

Then, the rigid-flat-bed experiment was conducted in order to analyse the turbulence characteristics of flow in the absence of topographically driven patterns ("initial flow"). During this experiment, the vertical, stream-wise and transverse flow velocity components were measured along five verticals of 17 measurement cross-sections (sections C÷Y of Fig. 1), selected in such a way as to cover the wavelength of the bed-forms. The first four sections (C, E, K and F) were spaced about 50 cm or so apart; from section F to section Y the distance between two consecutive sections was of 20 cm.

Measurements of the stream-wise and transverse flow velocity components was carried out using a 2D side-looking probe Acoustic Doppler Velocimeter (ADV) (Lemmin and Rolland 1997). The sampling frequency rate was F_s = 25 Hz. The vertical flow velocity component was measured through the DOP2000. The prin-

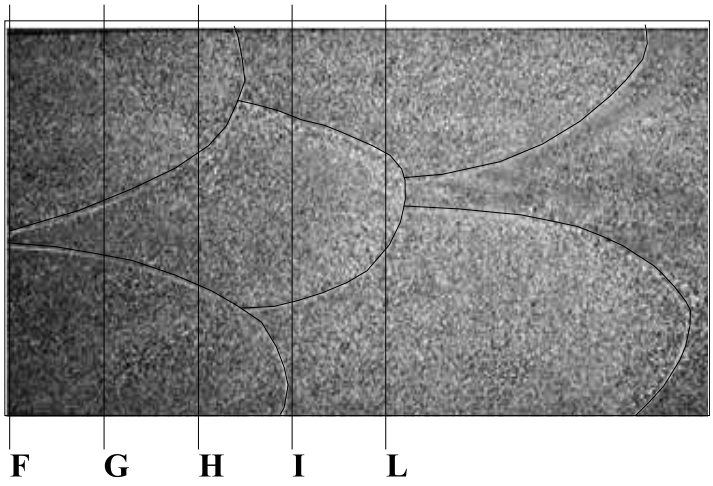

Fig. 2. Bed topography at the end of mobile bed experiment

ciple of functioning of both instruments is based on the Doppler effect. The ADV allows measurement of the local instantaneous flow velocity components for each measurement point, whereas the DOP2000 allows us to measure the instantaneous flow velocity profile along the direction of its probe. Details of the experimental setup and of measurement conditions are also reported in previous works (Termini 2005, Termini and Sammartano 2007).

Since our attention is particularly directed at the evolution of the bursting sequences occurring in the horizontal plane, which would be responsible for the alternate bars initiation (da Silva 2006, Termini and Sammartano 2007), in the present work only the longitudinal and transverse flow velocity components have been examined. Furthermore, the analysis concerns only the channel reach between sections F and L (see Fig. 1), where the wavelength of bed-forms was clearly distinguishable. In particular, section F is located a little upstream of the deposition side of two lateral bars; section L is near the crest of the central bar (see Fig. 2).

3. Data Analysis

3.1. Flow Velocity Field

First, the time series of the flow velocity components collected for each measurement point during the rigid-flat-bed experiments were examined. As an example, Fig. 3 shows the time series of the stream-wise component ($u_1(z,t)$) and of the transverse component ($u_2(z,t)$) (taken positive according to the reference system of Fig. 1) at $z = 1.0$ cm (z = distance of measurement point from the bed) of sections G and I along measurement longitudinal axes 1 and 3 (see Figure 1). From Fig. 3 the presence of numerous low frequency fluctuations can be observed in

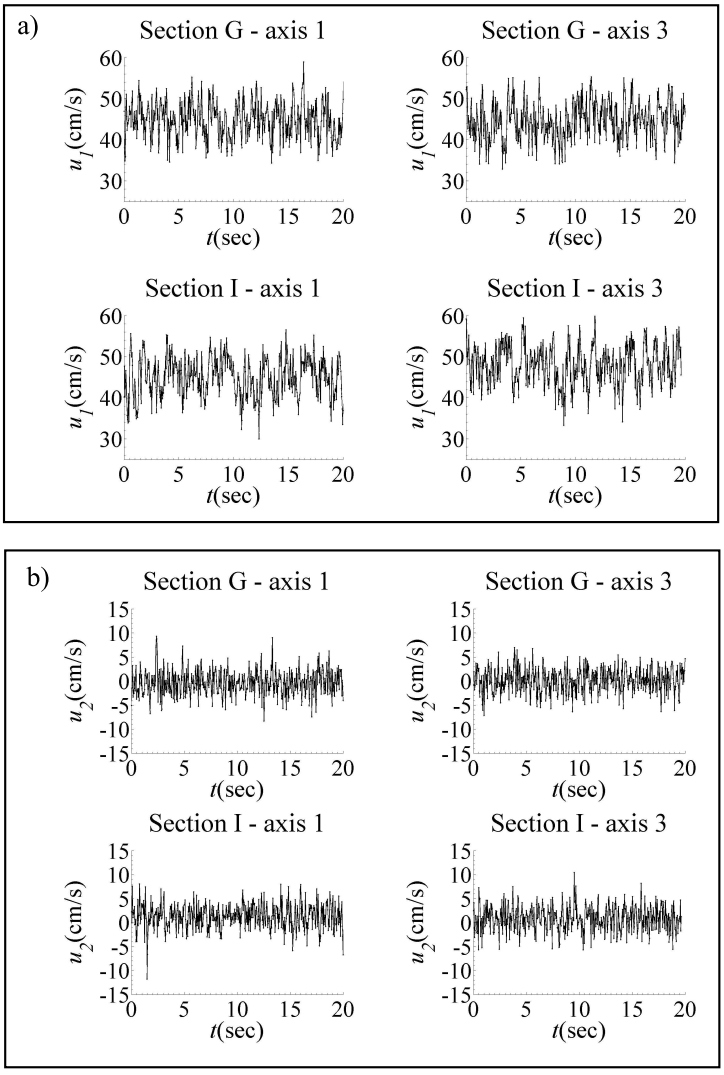

Fig. 3. Time series of flow velocity components at $z = 1.0$ cm of sections G and I: a) stream-wise component, $u_1(z, t)$; b) transverse component, $u_2(z, t)$

both stream-wise and transverse directions. Low frequency fluctuations are more evident at channel axis (axis 3) of section G (i.e. between the diagonal front of the lateral bars observed at the end of the mobile-bed experiment – see Fig. 2) and near the bank (axis 1) of section I (i.e. downstream the crest of the lateral bed forms – see Fig. 2). These low frequency fluctuations could be caused by the presence of low-speed regions of flow along the observed channel reach.

In Fig. 4 the horizontal distributions of the time-averaged stream-wise velocity component, $U_1(z)$, measured at $z = 1.0$ cm in sections F, G, H, I, L are reported. It can be observed from Fig. 4 that, in sections F and G, the horizontal distributions

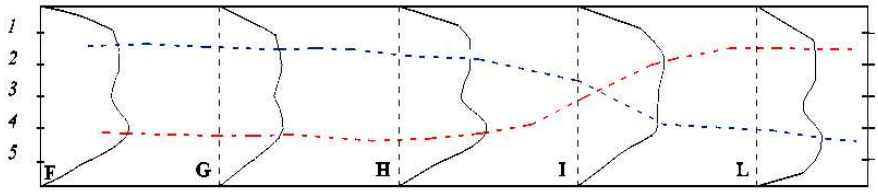

Fig. 4. Horizontal distributions of $U_1(z)$ at $z = 1.0$ cm

have a reduced axial velocity and two peak values near the banks. Thus, they contain inflection points and are unstable. The peak values shift downstream along the considered channel reach and, in section I, a peak value is found near the channel axis. This behavior could be related to the formation of pairs of counter-rotating vortices associated with bursting (Berkooz et al 1993, Pope 2000).

The power spectra of the stream-wise and transverse velocity components at $z = 1.0$ cm of sections F, G, H, I and L (axis 3) are reported, against the normalized frequency $F_n = Freq/F_s$ (with $Freq$ being the analysis frequency), in Fig. 5 and in Fig. 6 respectively.

The power spectra were obtained through the Fast Fourier Transform (FFT) technique (Pope 2000). From these figures it can be observed that for both velocity components, the higher peak values are found in sections F and G; in section I, an evident peak value also occurs for low frequencies. As Fig. 5 shows, for the stream-wise component, peak spectral values occur for very low frequencies ($<< 0.2$); for the transverse component (Fig. 6), the higher peaks occur for values of frequency little greater than those for stream-wise component.

3.2. Turbulent Fluctuation Components and Methodology of Analysis

The instantaneous turbulent fluctuation components have been estimated as deviations of the instantaneous flow velocity components from the corresponding time-averaged velocity component:

$$u_i'(z,t) = u_i(z,t) - U_i(z), \quad i = 1,2. \tag{1}$$

The knowledge of the turbulent fluctuation components allowed us to analyze the occurrence of turbulent events. It has been taken into account that the turbulent structures occur at different positions and times maintaining a common coherent pattern. Each turbulent event is distinguished by the direction of the instantaneous fluctuation components $u_1'(z,t)$ and $u_2'(z,t)$: ejection occurs when low-speed fluid ($u_1'(z,t) < 0$) moves far from the wall ($u_2'(z,t) > 0$); sweep event occurs when high-speed fluid ($u_1'(z,t) > 0$) moves toward the wall ($u_2'(z,t) < 0$); inward interactions occurs when low-speed fluid ($u_1'(z,t) < 0$) moves toward the wall ($u_2'(z,t) < 0$);

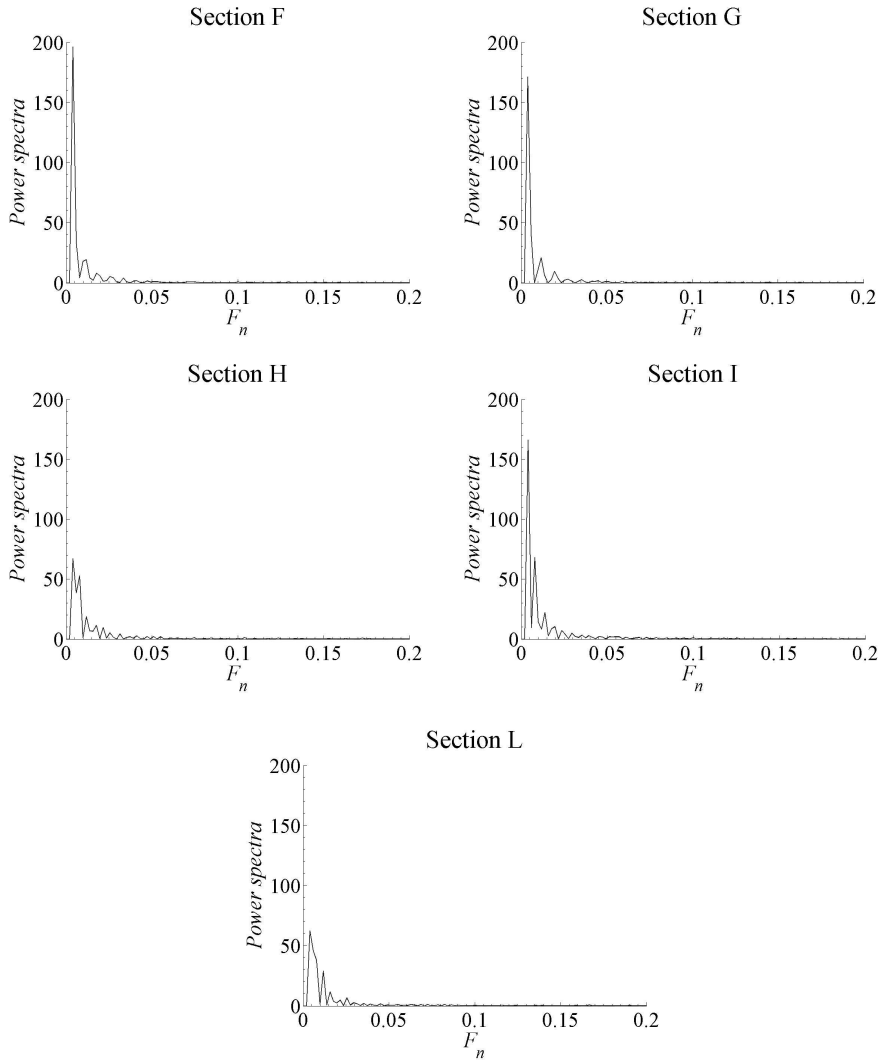

Fig. 5. Power spectra of stream-wise velocity component $u_1(z,t)$

outward interactions occurs when high-speed fluid ($u_1'(z,t) > 0$) arises far from the wall ($u_2'(z,t) > 0$). Thus, the qualitative description of turbulent events has been operated according to the sign of the turbulent fluctuation components and, for each measurement point, the instantaneous product $u_1'u_2'$, representing the Reynolds momentum flux, has been estimated. Negative values of the Reynolds momentum flux correspond to ejection and sweep events, whereas positive values of Reynolds momentum flux correspond to outward interactions (burst) and inward interactions. Both ejection and sweep events produce turbulent energy; outward and inward interactions determine energy dissipation (Pope 2000).

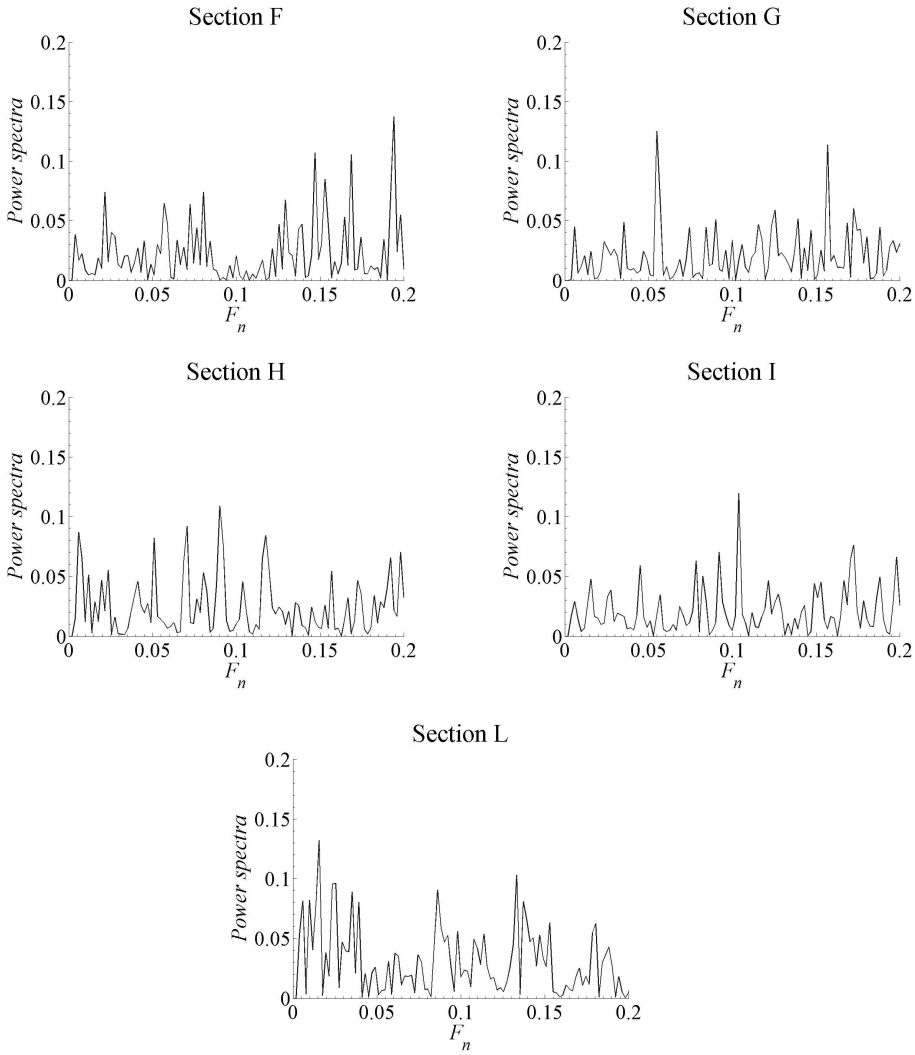

Fig. 6. Power spectra of transverse velocity component $u_2(z,t)$

The sign of the instantaneous Reynolds momentum flux was analyzed through conditioned quadrant analysis (Lu and Willmarth 1973, Nezu and Nakagawa 1993).

3.3. Conditioned Quadrant Analysis and Occurrence Frequency of Each Event

The instantaneous plane $u_1' - u_2'$ has been divided into four quadrants, so that each quadrant represents on average a turbulent event (see Fig. 7): quadrant I – outward interaction ($u_1'(z,t) > 0$ and $u_2'(z,t) > 0$); quadrant II – ejection ($u_1'(z,t) < 0$ and

$u_2'(z,t) > 0$); quadrant III – inward interaction ($u_1'(z,t) < 0$ and $u_2'(z,t) < 0$); quadrant IV – sweep ($u_1'(z,t) > 0$ and $u_2'(z,t) < 0$).

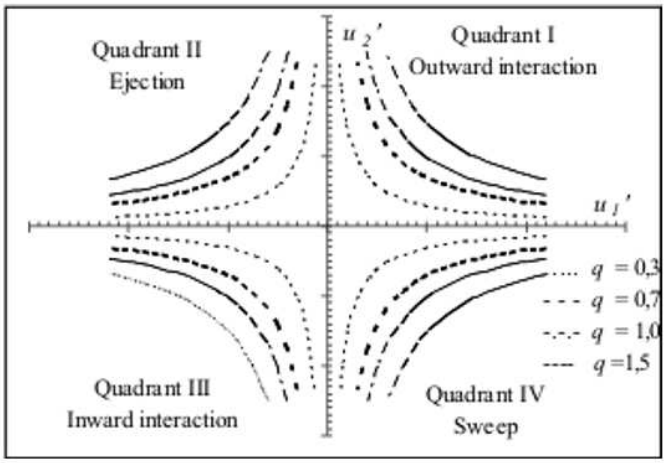

Fig. 7. Excluding hole regions

According to previous works (Nezu and Nakagawa 1993, Cellino and Lemmin 2004), in order to isolate the contribution of extreme events within each quadrant, a hyperbolic excluding hole has been defined on the instantaneous plane $u_1' - u_2'$. This excluding hole is bounded by the curves:

$$\left|u_1'(z,t) \cdot u_2'(z,t)\right| = q \cdot \sqrt{\overline{u_1'(z,t)}^2} \cdot \sqrt{\overline{u_2'(z,t)}^2}, \tag{2}$$

where q represents the threshold level. The over-bar indicates the time averaged value.

On the other hand, previous analyses conducted using the same flow velocity data with $q = 0$ (Termini and Sammartano 2007) have shown that when no excluding hole is considered, the occurrence of each event is not clearly distinguishable.

Thus, for each measurement point, the instantaneous Reynolds stress $u_1'u_2'$ has been filtered by a discriminating function $I_k(z,t)$ (where the index k = I, II, III, IV indicates the quadrant where the generic turbulent event falls). For each event, the discriminating function has been defined as follow:

$$
\begin{aligned}
I_I(z,t) &= \begin{cases} 1, & \text{if } u_1'(z,t) > 0;\ u_2'(z,t) > 0 \\ & \text{with excluding hole defined by Eq. (2)} \\ 0, & \text{otherwise;} \end{cases} \\
I_{II}(z,t) &= \begin{cases} 1, & \text{if } u_1'(z,t) > 0;\ u_2'(z,t) > 0 \\ & \text{with excluding hole defined by Eq. (2)} \\ 0, & \text{otherwise;} \end{cases} \\
I_{III}(z,t) &= \begin{cases} 1, & \text{if } u_1'(z,t) > 0;\ u_2'(z,t) > 0 \\ & \text{with excluding hole defined by Eq. (2)} \\ 0, & \text{otherwise;} \end{cases} \\
I_{IV}(z,t) &= \begin{cases} 1, & \text{if } u_1'(z,t) > 0;\ u_2'(z,t) > 0 \\ & \text{with excluding hole defined by Eq. (2)} \\ 0, & \text{otherwise.} \end{cases}
\end{aligned}
\tag{3}
$$

The discriminating functions defined by Eq. (3) allow for identification of the regions contributing to turbulent events. The dimension of such regions and, thus, of the corresponding excluding hole depends on the value of the threshold level q. In general, the determination of q is more or less arbitrary. Very small values of q allow us to select either both strong and weak events; large values of q allow us to select only strong events.

The main purpose of the present analysis is to isolate the strongest events and to identify the frequency of occurrence by progressively eliminating the weak events. Thus, the analysis is conducted by assuming four different threshold levels q (q = 0.3, 0.7, 1.0, 1.5). The excluding holes corresponding to such threshold levels are shown in Fig. 7. From this figure it can be observed that as the values of the threshold level q increase, the corresponding contributing regions become smaller. As a consequence, the total number of couples $u_1' - u_2'$ considered for the analysis could be greatly reduced.

For each considered threshold level and for each measurement point, the occurrence frequency of the event falling in k-th quadrant, $f_k(z)$ (k = I, II, III, IV), has been estimated as:

$$
f_k(z) = \frac{N_{k,z}}{\sum_{t=0}^{T} I_I(z,t) + \sum_{t=0}^{T} I_{II}(z,t) + \sum_{t=0}^{T} I_{III}(z,t) + \sum_{t=0}^{T} I_{IV}(z,t)}, \tag{4}
$$

where $N_{k,z} = \sum_{t=0}^{T} I_k(z,t)$ is the number of occurrences of a turbulent event in k-th quadrant, T is the measurement time length.

As an example, in Fig. 8 the histograms of the values of $f_k(z)$, estimated at z = 1.0 cm for each considered threshold level q and for each section along axis 1 (near the bank) and along axis 3 (channel axis), are shown. It can be observed that: for low values of q (q = 0.3), along axis 1 high occurrence frequencies which fall

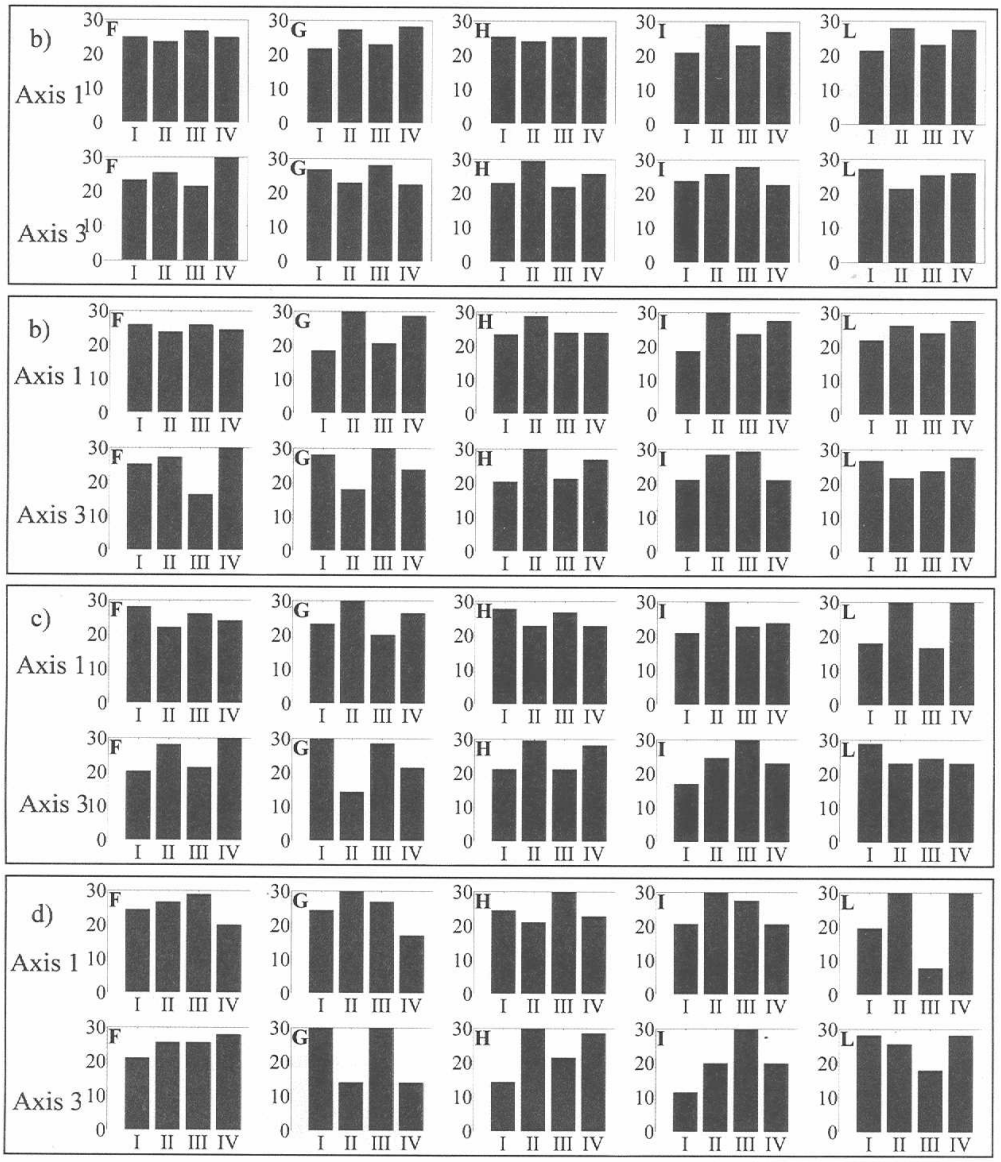

Fig. 8. Histograms of conditioned events: a) q = 0.3; b) q = 0.7; c) q = 1.0; d) q = 1.5

in quadrants I (k = I) and III (k = III) occur in sections F and H; the occurrence frequency assumes high values in quadrants II (k = II) and IV (k = IV) in both sections I and L. Along the channel axis (axis 3), the occurrence frequency assumes high values in quadrants I and/or III for section I; higher frequencies which fall in quadrants II and/or IV occur in sections F, H and L. For both axes, in section G the occurrence frequency seems to assume very similar values in each quadrant.

As the threshold level q increases ($q = 0.7 < 1$), the histograms seem to show the occurrence frequency of each event more clearly than in previous cases. This is particularly evident in section G, where higher values of the occurrence frequency are found in quadrants II and IV along axis 1 and in quadrants I and III along axis 3. But the behavior of turbulent events is not clearly distinguishable in section I, yet.

For high values of the threshold level ($q = 1$ and $q = 1.5$) the distinction of each event is evident further on. It can be observed that near the bank (axis 1), a high occurrence frequency of events with k = II and k = IV are found in sections G and I; events with k = I and k = III occur in sections F and H. In section L the histograms show high occurrence frequency in the same k-th quadrants as observed in section I. Basically, along both axes, events of quadrant II and/or IV occur in sections at a spacing of 40 cm. Furthermore, the evolution of turbulent events seems to alternate, passing from axis 1 (near the bank) to axis 3 (at channel axis), as well as the bars observed on the bed. The behavior observed in Fig. 8 confirms that values of threshold level $q \geq 1$ allow us to distinguish clearly the frequency of occurrence of each event, also if the total number of the considered couples $u'_1 - u'_2$ is necessarily reduced. Therefore, in the following analysis, the threshold level $q = 1$ has been used. It has been considered as a good compromise between a clear distinction of the events and an acceptable number of considered couples $u'_1 - u'_2$.

Thus, the instantaneous turbulent fluctuation components, $u'_1(z,t)$ and $u'_2(z,t)$, have been filtered by considering the excluding hole identified by the threshold level $q = 1$. The filtered time series $\hat{u}'_1(z,t)$ and $\hat{u}'_2(z,t)$ have been obtained as:

$$\hat{u}'_1(z,t); \hat{u}'_2(z,t) = \begin{cases} \left|u'_1(z,t) \cdot u'_2(z,t)\right| = q \cdot \sqrt{\overline{u'_1(z,t)}^2} \cdot \sqrt{\overline{u'_2(z,t)}^2} \\ q = 1 \end{cases} . \tag{5}$$

3.4. Probability Density Function

In order to identify the probability of occurrence of each event, the joint probability density function of filtered couples $(\hat{u}'_1(z,t), \hat{u}'_2(z,t))$, $P_{12}(z)$, has been estimated as:

$$P_{12}(z) = A_{12} \cdot \exp\left[B_{12} \cdot \left(\frac{\hat{u}'_1(z,t)^2}{\hat{u}'_1(z,t)^2} - 2 \cdot \frac{\rho_{12} \cdot \hat{u}'_1(z,t)\hat{u}'_2(z,t)}{\left[\overline{\hat{u}'_1(z,t)^2}\ \overline{\hat{u}'_2(z,t)^2}\right]^{0.5}} + \frac{\hat{u}'_2(z,t)^2}{\hat{u}'_2(z,t)^2} \right) \right], \tag{6}$$

where

$$A_{12} = \left[4\pi^2 \cdot \overline{\hat{u}'_1(z,t)^2 \hat{u}'_2(z,t)^2} \cdot \left(1 - \rho_{12}^2\right)\right]^{-0.5}, \quad B_{12} = \frac{-0.5}{1 - \rho_{12}^2}$$

and

$$\rho_{12} = \overline{\hat{u}'_1(z,t) \cdot \hat{u}'_2(z,t)} \cdot \left[\overline{\hat{u}'_1(z,t)^2 \hat{u}'_2(z,t)^2}\right]^{-0.5}.$$

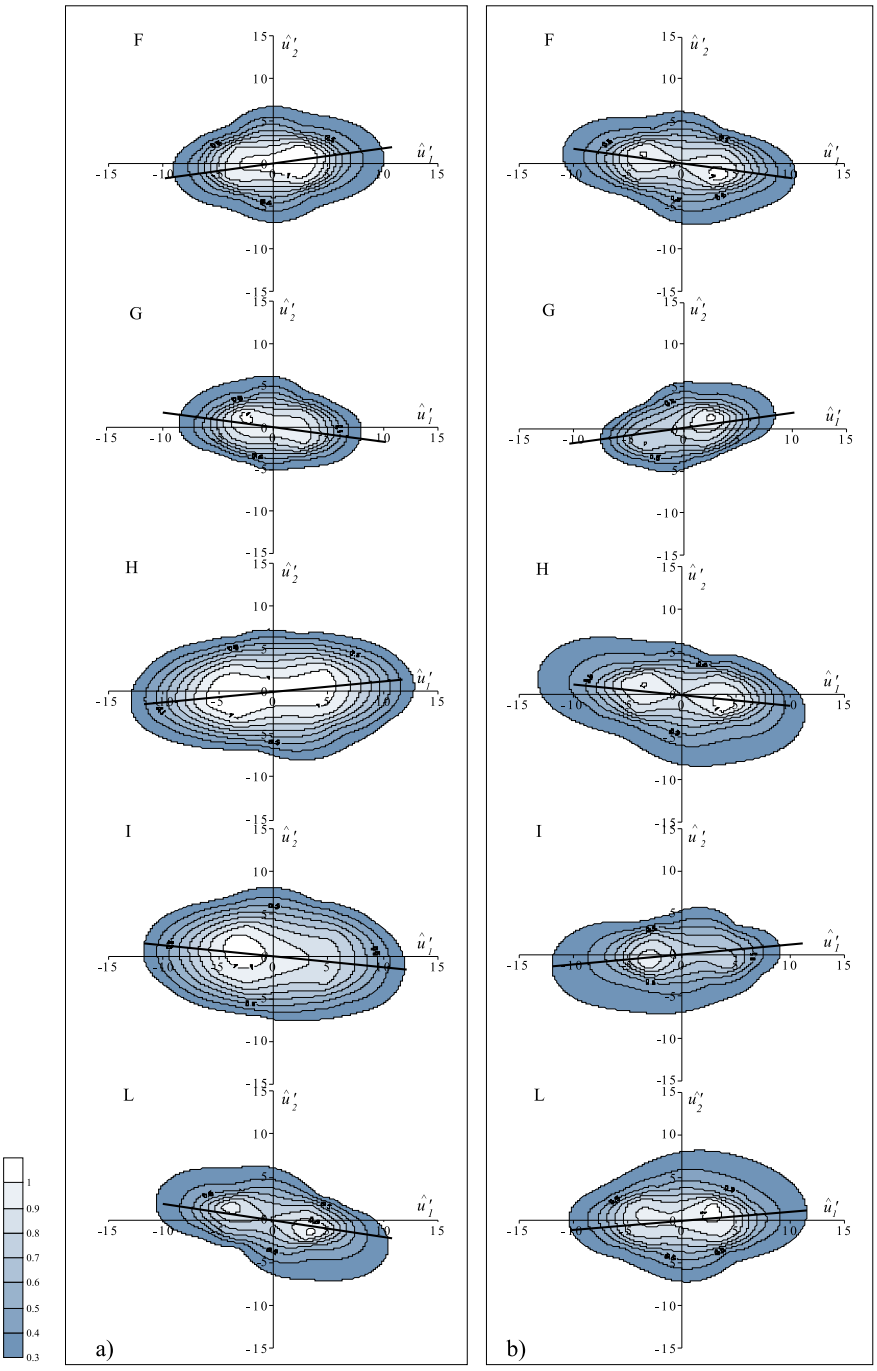

Fig. 9. $P_{12}(z)$ contours-lines: a) axis 1; b) axis 3

The distribution of $P_{12}(z)$ on the plane $\hat{u}'_1 - \hat{u}'_2$ is represented by an ellipse whose long axis is rotated according to the more frequent event occurring in the considered measurement point.

Fig. 9 shows the contour-lines of $P_{12}(z)$ estimated (at $z = 1.0$ cm) along axes 1 and 3 of the channel reach F-L. It can be observed that near the bank (axis 1) the long axis of the ellipse is rotated so as to fall in the second and in the fourth quadrants in sections G, I and L; in sections F and H the long axis of the ellipse falls in quadrants I and III. In particular, along axis 1 in both sections G and I, the peak value of the probability density is found in quadrant II; in section L the peak value is in quadrant IV. Consequently, in sections G and I ejection event seems to occur; in section L a sweep event seems to develop. Along the channel axis (axis 3), the long axis of the ellipse of each section assumes the direction opposite to that observed in the same section near the bank: in sections F and H the long axis is rotated so as to fall in the second and fourth quadrants; the peak value falls in the fourth quadrant (sweep event). In sections G, I and L the long axis falls in quadrants I and III. In sections G and L, the peak value is found in quadrant I (outward interaction); in section I it occurs in quadrant III (inward interaction).

On the basis of the observed probability distributions, it can be supposed that near the bank an eddy forms near section F, and it evolves with an ejection event in section G; because of the interaction with the mean flow (section H), a new eddy forms (section I) and at section L the sweep event occurs. From Fig. 2 it can be observed that ejection events occur in sections where erosion holes form on the bed, and outward interactions where deposition occurs.

3.5. Analysis of Correlation Functions and Ejection/Sweep Event Identification

In order to identify the time-space evolution of the observed turbulent structures, the correlation functions of the instantaneous bed level data have been estimated both in temporal and in spatial domains.

The correlation coefficient, ρ_{12}, between the filtered time series $\hat{u}'_1(z,t)$ and $\hat{u}'_2(z,t)$ for k = II, IV, has been determined as:

$$\rho_{12}(\tau) = \frac{\overline{\hat{u}'_1(z,t) \cdot \hat{u}'_2(z,t+\tau)}}{\sqrt{\overline{\hat{u}'_1(z,t)^2} \cdot \overline{\hat{u}'_2(z,t)^2}}}, \tag{7}$$

where τ is the time lag.

Fig. 10 shows the correlation functions estimated for each considered section along both axes. It can be observed that at time lag $\tau = 0$, the correlation is negative. As the time lag increases, higher and more frequent peaks occur in sections G and I along axis 1, and in sections F and H along axis 3.

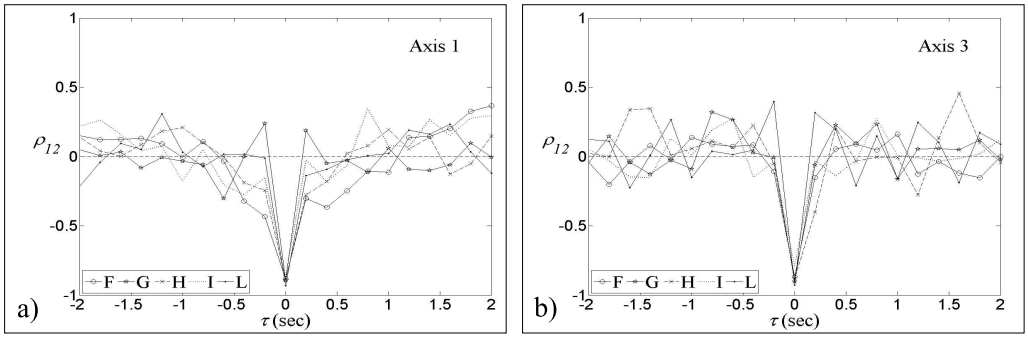

Fig. 10. Correlation between the filtered time series $\hat{u}'_1(z,t)$ and $\hat{u}'_2(z,t)$ with k = II, IV: a) axis 1; b) axis 3

Furthermore, for the same time lag, the peak values observed in sections G and I along axis 1 correspond to the peak values observed in sections F and H along axis 3. Such behavior confirms that ejection and sweep events occur both near the bank (axis 1) and at the channel axis (axis 3), alternating in sections spaced at 40 cm.

Thus, the conditional sampling technique (Nezu and Nakagawa 1993) has been applied to recognize the average information related to the development of the considered turbulent events along the analysed channel reach. The conditional sampling of the filtered time series $\hat{u}'_i$ ($i = 1, 2$), and its averaging, has been estimated as:

$$< \hat{u}'_i(\Delta x, z, \tau) >= \frac{\sum\limits_T \left\{ \left[\hat{u}'_i(z, t+\tau) \right]_S \cdot [I_k(z,t)]_{S_0} \right\}}{\sum\limits_T [I_k(z,t)]_{S_0}}, \tag{8}$$

where the subscripts S_0 and S indicate the initial section and the detected section respectively, Δx is the spatial lag, the symbol <> indicates the conditioned average value.

On the basis of the aforementioned considerations (see Fig. 9), a spatial lag Δx = 40 cm has been considered. The averaged pattern of the conditioned variables $< \hat{u}'_1(40, z, \tau) >$, $< \hat{u}'_2(40, z, \tau) >$ has been analysed by assuming a variable time lag.

In order to investigate the occurrence of ejection and sweep events, it has been assumed k = II, IV. Furthermore, section G has been considered as the initial section (S_0 = G) and section I as the detected section (S = I) along axis 1; it has been assumed S_0 = F and S = H along axis 3.

As an example, the conditionally averaged patterns of components $< \hat{u}'_1(40, 1, \tau) >$, $< \hat{u}'_2(40, 1, \tau) >$, associated with ejection and sweep events, are plotted against the time lag τ in Fig. 11. It can be observed from this graph that peak values occur with temporal length of about $0.6 \div 0.8$ sec. Along both axes, positive peaks of the conditionally averaged $< \hat{u}'_1(40, 1, \tau) >$ correspond to negative peaks of condition-

ally averaged $< \hat{u}'_2(40, 1, \tau) >$, and vice-versa. Such patterns confirm that ejection and sweep events occur in sections G and I along axis 1, and in sections F and H along axis 3.

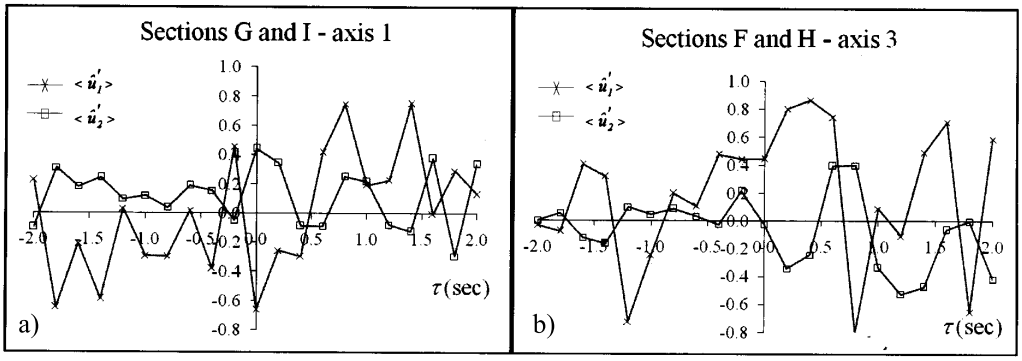

Fig. 11. Averaged patterns of $< \hat{u}'_1(40, 1, \tau) >$, $< \hat{u}'_2(40, 1, \tau) >$ (k = II, IV): a) axis 1; b) axis 3

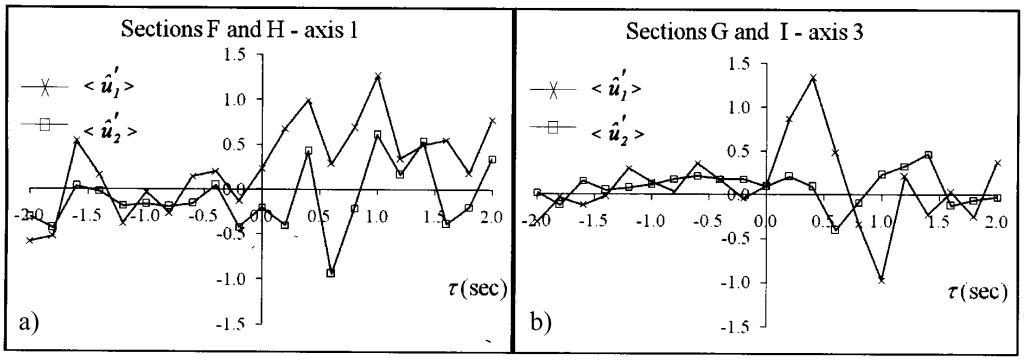

Fig. 12. Averaged patterns of $< \hat{u}'_1(40, 1, \tau) >$, $< \hat{u}'_2(40, 1, \tau) >$ (k = I, III): a) axis 1; b) axis 3

Then, in order to investigate the occurrence of inward and outward interactions, the averaged patterns of the conditioned variables $< \hat{u}'_1(40, 1, \tau) >$, $< \hat{u}'_2(40, 1, \tau) >$ have been estimated by assuming k = I, III. In this case, section F has been considered as the initial section along axis 1 and section G as the initial section along axis 3; sections H and I have been considered as the corresponding detected sections. The estimated conditionally averaged patterns are plotted against τ in Fig. 12. It can be observed that along both axes the signs of the peaks of the averaged patterns of the conditioned variables $< \hat{u}'_1(40, 1, \tau) >$, $< \hat{u}'_2(40, 1, \tau) >$ are in agreement. Also, in this case, the peak values occur with a temporal periodicity of about $0.6 \div 0.8$ sec.

The observed trend confirms that events of inward and/or outward interactions occur in sections F and H along axis 1, and in sections G and I along axis 3.

4. Conclusions

In the present work, the occurrence of turbulent events (inward interaction, ejection, sweep and burst) along a straight flume has been verified through conditioned quadrant analysis. In order to isolate the strongest events and to identify the frequency of occurrence by progressively eliminating the weak events, four values of the threshold level q have been assumed.

The analysis has highlighted that for the examined conditions, the threshold level $q = 1$ is a good compromise between a clear distinction of the events and an acceptable number of data considered for the analysis.

In order to define the probability of occurrence of each event, the joint density function of the filtered couples $(\hat{u}'_1(z,t), \hat{u}'_2(z,t))$ has been determined. It has been verified that, on the plane $\hat{u}'_1 - \hat{u}'_2$, the long axis of the ellipse, representing the probability density distribution, is oriented so as to fall in quadrants II and IV (ejection and/or sweep events) in sections spaced at almost 40 cm. The observed behavior seems to be alternated between axis 1 (near the bank) and axis 3 (channel axis). The time-space evolution of the observed turbulent structures has been analyzed both by applying the conditional sampling technique, recognizing the average information related to their development, and through the correlation functions of the filtered time series $\hat{u}'_1(z,t), \hat{u}'_2(z,t)$. Both the analyses have confirmed that ejection and sweep events occur in alternation both near the bank and at the channel axis, with the same spatial scale of the bed forms observed on the bed. In particular, such events have been found in sections where the scour holes of the bars occur.

References

Berkooz G., Holmez P. and Lumley J. L. (1993) The proper orthogonal decomposition in the analysis of turbulent flows, *Ann. Rev. Fluid Mech.*, **25**, 539–575.

Cantwell B. J. (1981) Organized Motion in Turbulent Flow, *Ann. Review Fluid Mechanics*, 457–515.

Corino E. R. and Brodkey R. S. (1969) A visual investigation of the wall region in turbulent flow, *Journal of Fluid Mechanics*, **37**, 1–30.

Cellino M. and Lemmin U. (2004) Influence of coherent flow structures on the dynamics of suspended sediment transport in open-channel flow, *Journal of Hydraulic Engineering*, 1077–1088.

Da Silva A. M. F. (2006) On why and how river meander, *Journal of Hydraulic Research*, **44** (5), 579–590.

Holmes R. R. and Garcia M. H. (2008) Flow over bedforms in a large sand-bed river: a field investigation, *Journal of Hydraulic Research*, **46** (3), 322–333.

Jackson R. (1976) Sedimentological and fluid-dynamic implications of the turbulent bursting phenomenon in geophysical flows, *Journal of Fluid Mechanics*, **77**, part 3, 531–560.

Kaftori D., Hetsroni G. and Bnerjee S. (1995) Particle behavior in the turbulent boundary layer II. Velocity and distribution profiles, *Physics of Fluids*, **7**, 1107–1121.

Kline S. J. Reynolds W. C., Schraub F. A., Runstadler P. W. (1967) The structure of turbulent boundary layers, *Journal of Fluid Mechanics*, **30** (2), 741–773.

Lemmin U. and Rolland (1997) Acoustic Velocity profiler for laboratory and Field studies, *Journal of Hydraulic Engineering*, **123** (12), 1089–1097.

Lu S. S. and Willmarth W. W. (1973) Measurements of the Reynolds stress in a turbulent layer, *Journal of Fluid Mechanics*, **60** (3), 481–511.

Nelson J. M., Shreve R. L., Mclean S., Drake T. G. (1995) Role of near-bed turbulence structure in bed load transport and bed form mechanics, *Water Resources Research*, **31** (5), 2071–2086.

Nezu I. and Nakagawa H. (1993) *Turbulence on open channel flows*, A. A. Balkema Publishers, Rotterdam, the Netherlands.

Nezu I. and Rodi W. (1986) Open-channel flow measurements with a laser Doppler anemometer, *Journal of Hydraulic Engineering*, ASCE, **112**, 335–355.

Nino Y. and Garcia M. H. (1996)Experiments on particle-turbulence interactions in the near-wall region of an open channel flow: implications for sediment transport, *Journal of Fluid Mechanics*, **326**, 285–319.

Pope S. B. (2000) *Turbulent flows*, Cambridge University Press.

Rashidi M., Hetsroni G. and Banerjee S. (1990) Particle-turbulence interaction in a boundary layer, *International Journal of Multiphase Flow*, **16** (6), 935–949.

Shen W. and Lemmin U. (1999) Application of an acoustic particle flux profiler in particle-laden open-channel flow, *Journal of Hydraulic Research*, **37**, 407–419.

Shvidchenko A. B. and Pender G. (2001) Macroturbulent structure of open-channel flow over gravel beds, *Water Resources Research*, **37** (3), 709–719.

Termini D. (2005) Experimental investigation on the horizontal turbulence and the bed deformation: preliminary results, *CD-Proceeding International Symposium on Stochastic Hydraulics – IAHR Congress*, 23–24 May, Nijmegen – The Netherlands.

Termini D. and Lo Re C. (2006) Analysis of the relation between the flow "horizontal" turbulence and the bed deformation, *Proceeding International Symposium on sediment Dynamics and the Hydromotphology of Fluvial Systems* – Dundee (Scotland) 3–7 July, 73–79.

Termini D. and Sammartano V. (2007) Analysis of the role of turbulent structure in bed-forms formation in a rectilinear flume, *32nd Congress of IAHR, "Harmonizing the Demands of Art and Nature in Hydraulics"* – Venice, Italy 1–6 July.

Utami T. and Ueno T. (1991) Experimental Study on the Compound meandering Channel Flow using Flow Visualization and picture processing, *Journal of Hydroscience and Hydraulic Engrg.*, **9** (1), 1–10.

Yalin M. S. (1992) *River Mechanics*, Pergamon Press, London.

Yalin M. S. and da Silva A. F. (2001) *Fluvial Processes*, IAHR Monograph, Delft, The Netherlands.